Capturing the wetting state of an aged-carbonate core through pore-scale multiphase flow simulations

Tingting Wang[1], *Ying Da* Wang[1], *Chenhao* Sun[2], *James E.* McClure[3], *Peyman* Mostaghimi[1], *Ryan T.* Armstrong[1,*]

[1]School of Minerals and Energy Resources Engineering, University of New South Wales, Kensington, New South Wales, Australia
[2]State Key Laboratory of Petroleum Resources and Prospecting, China University of Petroleum, Beijing 102249, PR China
[3]Advanced Research Computing, Virginia Polytechnic Institute and State University, Blacksburg, VA, USA

Abstract. Recent state-of-the-art Digital Rock (DR) technology is becoming an important workflow to complement and expand laboratory data with realistic simulations over a wider parameter space. With DR technology, X-ray computed microtomography (micro-CT) images of rocks are commonly used for relative permeability simulations. However, currently no clear approach exists for the integration of realistic rock surface wetting conditions into DR simulations, even though it is well known that multiphase flow is significantly influenced by the surface wetting properties of rocks. Realistic DR simulations requires a fundamental understanding of wetting at the length scale at which interfaces are well resolved, which is currently lacking in the literature. To address this issue, we conducted 2-phase Lattice-Boltzmann simulations in a carbonate rock using a developed effective wetting model that captures the multi-scale nature of the micro-porous and macro-porous regions, which allows for spatially variable wetting conditions that mimic an aged-state core. Simulation phase morphologies are then compared to experimental studies for a clean-state and aged-state core imaged with micro-CT to evaluate the wetting model and corresponding simulation results. Overall, the proposed research is tailored to investigate the fundamental processes of wetting in porous media needed for multiphase flow DR simulations.

1 Introduction

Wettability in a broad sense refers to a surface property where in the presence of two immiscible fluids, one fluid preferentially wets the surface [1]. It is a surface property of a substance, which exists widely in nature[2]. Wettability is an important characteristic of the interaction between rock and fluids, which reflects the distribution of oil and water in a reservoir. It plays an important role in multiphase flow and can significantly influence oil recovery [3].

The Lattice Boltzmann Method (LBM) works well for simulating single-phase and multi-phase flows [4]. However, when simulating multiphase flow, how to effectively consider surface wettability is a crucial factor affecting simulation results [5]. Wettability is an important factor that influences the flow characteristics of fluids in porous media. It can influence many physical parameters of reservoir rocks, such as irreducible water saturation, residual oil saturation, relative permeability, and capillary pressure [6]. How to assign a realistic wetting condition for direct multiphase flow simulations remains an open question.

In the early stage of wettability research, according to the fact that the minerals that make up reservoir rocks are mostly hydrophilic the wetting state was considered largely water wet. Later, it was found that after the formation of an oil reservoir, the rock surface will contact oil for geological time, and the active substances in crude oil will adhere to the rock surface, which changes the rock surface from water wet to oil wet or intermediate wet [7]. Assuming that the reservoir rock is homogeneous, the wetting tendency of water or oil would be uniform on the rock surface. Uniform wetting could be oil wet, water wet, or intermediate wet. However, due to the rock heterogeneity, distribution of fluids, and complexity of the crude oil, the actual rock could appear heterogeneous wetting, showing that parts of the surface are water wet, while others are rendered intermediate or oil wet [3].

There are two common lab methods to age cores to a 'reservoir condition'. One is static aging [8], the other is dynamic aging [9]. After aging, the rock surface will have a wettability alteration and reach a more oil-wet condition than before. For either method the rock core is aged in crude oil at connate water saturation for an extended period. Rock surfaces in contact with oil are rendered oil wet or intermediate wet depending on the period of aging and properties of the crude oil. Of critical consideration is the acid content of the oil whereby more acidic oils are more active at rendering surfaces oil wet [10].

The wettability of rock is commonly characterized by an experimentally measured contact angle using the sessile drop technique [11]. However, this method can only describe the wettability of the pore surface at a specific location and cannot reflect the realistic wettability distribution in the pore space. In addition, contact angle measurements taken on a rock surface are an apparent contact angle at the length scale of the observation and do not necessarily reflect the intrinsic contact angle of a surface. Carbonate rocks, e.g., include micro-porous and macro-porous regions, apparent contact angle measurements are commonly taken at the macro-

* Corresponding author: ryan.armstrong@unsw.edu.au

pore length scale while the underlying microporous structure would influence the measurement [2].

Treiber et al. 1972 [12] show that approximately 80% of the more than 50 reservoirs they studied were moderately oil wet, i.e., contact angles from 120° to 140°. These moderately oil-wet systems are difficult to identify, and the wettability of core samples from these reservoirs can be easily altered inadvertently [13]. How to truly and completely reconstruct the pore space with its realistic wettability is still an important problem to be solved, which is more readily becoming a reality with the development of *in situ* contact angle measurements from X-ray computed microtomography images [14].

For carbonate rocks, AlRatrout et al. [15] measured *in situ* contact angles between immiscible fluids on segmented X-ray images, they found that for an aged sample, contact angles were more widely spread than water-wet conditions with values both less than and greater than 90°. They measured *in situ* contact angles of three samples (total of 595 million voxels) and reported a mean and standard deviation of 77°± 21° indicating a weakly water-wet condition with few oil-wet surfaces; 104°±26° showing a mixed-wet system with more oil-wet surfaces; and 94°±24° illustrating a mixed-wet system with contact angles ranging from water-wet to oil-wet. AlRatrout et al. [3] observed a wide range of contact angle values on flat calcite surfaces, the average contact angle values were 76°, 130°, and 141° for different wetting conditions.

Herein, we investigate a method to capture surface wettability in a digital rock model that mimics the realistic wettability of an aged-carbonate core. We take a targeted assignment of surface wettability, which can be changed from initially water wet to oil wet through the simulated contact of oil with the rock surface. After primary drainage, all rock surfaces in contact with oil are set to be oil wet, and all other surfaces remain water wet to mimic the aging process. Our proposition is that to what degree the oil-wet regions become oil-wet depends on the microporosity of the pore walls. Micropores retain water, and thus potentially remain water wet (to a degree) since the capillary pressure required to drain the microporosity is restrictively high. For validation, we compare pore-scale experimental images of fluids in an aged-carbonate core to those simulated under various wetting conditions. The Minkowski Functionals (MFs) are used to compare the fluid phase morphologies and contact angle measurements are used to understand the wetting condition and the influence that microporosity has on the apparent (effective) contact angle.

2. Materials and method

2.1 X-ray computed microtomography data

Two data sets were selected from the Digital Rocks Portal (https://www.digitalrocksportal.org/).

- Dataset 1: We used the Ketton image from DOI - 10.17612/P7HT11. The resolution of the image was 5 micrometres per voxel side using a laboratory-based X-ray micro-CT scanner [16].
- Dataset 2: We used the experiment data from the project DOI - 10.17612/3S3K-EE20. The images were obtained at a synchrotron facility during water injection in a mixed-wet sample [17]. The image resolution was 3.5 micrometres.

Dataset 1 comprises of greyscale and segmented multiphase images, but no images of experiments of mixed-wetting aged cores, while Dataset 2 does not contain an original greyscale image but does contain segmented multiphase images of an aged-carbonate core during an imbibition experiment. Dataset 2 was reported as a mixed-wet sample [17]; however, the experimental data shows an initial water saturation of 0.1% in the macropores.

2.2 Simulation

Two-phase Lattice Boltzmann Method (LBM) simulations were carried out on Dataset 1 and 2. The details of the implementation are provided by McClure et al. [18]. The mixed wetting nature of these cores was mapped onto the surface of the solid voxels by identifying whether solid voxels are in contact with water or oil after a primary drainage simulation. A workflow for the assignment of contact angles is provided in Figure 1. We assume that after primary drainage, the phase distributions are static, and over time, the wettability of the surfaces in contact with oil are altered, i.e., dynamic aging of the surface is not considered. The wettability of the domain thus becomes mixed wet, with surfaces in contact with water remaining water wet, and surfaces in contact with oil becoming oil wet. The exact contact angles to be assigned to the water-wet and oil-wet regions are discussed in Section 3.

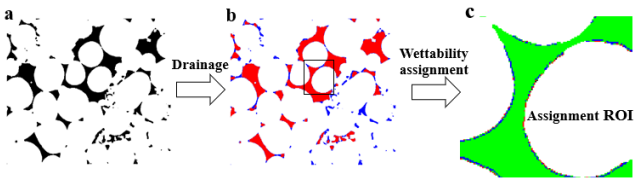

Fig. 1. The workflow for the assignment of contact angles; a is the binary image; b is the image after drainage; c is the Region-of-interest (ROI) image after wettability assignment.

In our implementation of LBM, the wetting of a surface to the two fluids present (defined as -1 and +1) can be defined as a scalar value α, ranging from -1 to +1. This is equivalent to assuming that the solid phase and surface of the solid is an immobile phase with an affinity to the two fluids proportional to the distance of α to fluid -1 and fluid +1. This automatically recovers the expected contact line and contact angle behaviour at both dynamic and static conditions [18]. On a flat surface of affinity α, the static contact angle can be defined as

$$\cos\theta = \alpha \, . \qquad (1)$$

This angle can be considered as an effective (or apparent) contact angle at the pore scale.

All simulations were conducted at a Capillary number of 1×10^{-5}.

2.3 Contact Angle Models

We consider two methods for assigning the effective contact angle for the water-wet and oil-wet regions. Model (1) Uniform Wetting: we assume that the surfaces are smooth, impermeable, and homogenous. Therefore, a single effective contact angle is assigned to the oil-wet regions and likewise for the water-wet regions. Model (2) Cassie-Baxter Wetting: we assume that the grain surfaces are microporous and retain water which thereby influences the effective contact angle. This is reasonable for carbonate rocks given that the capillary pressure required to penetrate the microporosity during aging is typically not exceeded in experiments nor under geological conditions.

We follow the microporosity analysis method presented by Lin et al. [14]. The CT value of a voxel is proportional to the voxel density, in this way we can define the solid fraction on a per voxel basis as

$$\emptyset_s = \frac{CT_{voxel} - CT_{macropores}}{CT_{grain} - CT_{macropores}}, \quad (2)$$

where $\emptyset_s$ is voxel solid fraction, CT_{voxel} is the CT number of each voxel, $CT_{macropores}$ is the average CT value of macropores, and CT_{grain} is average CT value of the grains.

Based on the assumptions for Method (2) during aging the fraction of the carbonate rock surface that is exposed to oil depends on the microporosity. This means that only a fraction of a given voxel is rendered oil wet. The Cassie-Baxter model [2] provides a means to define this condition as

$$\cos\theta_E = \emptyset_s \cos\theta_Y + (1 - \emptyset_s), \quad (3)$$

where $\emptyset_s$ is the carbonate voxels solid fraction in contact with the oil surface, θ_Y is the intrinsic contact angle of a solid carbonate surface, and θ_E is the effective contact angle observed in a pore-scale image.

2.4 Minkowski Functionals

The Minkowski Functionals (MF) are geometric measures of size based on set theory (Serra 1983), which are commonly used in porous media research [19]. By considering the surface δX of phase (X) embedded in Euclidean space (Ω), the MFs are $d+1$ functionals, where d is the dimension of Ω. In three dimensional (3D) space, the MF are effectively volume, surface area, integral mean curvature, and Euler characteristic. M_0 is the first functional and represents the total volume of X. M_1 is the second functional and represents the integral measure of the surface area of X, defined as

$$M_1(X) = \int_{\delta X} ds, \quad (4)$$

where δX is the entire surface and ds is the surface element on X. M_2 is the third functional and represents the integral of mean curvature of the entire surface, which is defined as

$$M_2(X) = \int_{\delta X} \left[\frac{1}{r_1} + \frac{1}{r_2}\right] ds, \quad (5)$$

where r_1 and r_2 are the principal radii of curvature of surface element ds. M_3 represents the integral of Gaussian curvature of the entire surface, which is defined as

$$M_3(X) = \int_{\delta X} \left[\frac{1}{r_1 \times r_2}\right] ds = 4\pi\chi(X), \quad (6)$$

where $\chi(\delta X)$ is the Euler characteristic of the bounding surface and $\chi(X)$ is the Euler characteristic of phase X (Ohser and Mücklich 2000; Michielsen and De Raedt 2001). The Euler characteristic can also be described by isolated objects (N), redundant loops (L) and cavities (O), defined as

$$\chi(X) = N - L + O. \quad (7)$$

Equation (7) provides a more direct understanding of Euler number, i.e., a system with more loops has higher connectivity and more negative Euler number.

3. Results and discussions

For Model (2), we considered θ_Y = 130° for oil-treated surfaces and θ_Y = 40° of untreated surfaces. For Model (1), we considered a uniform contact angle of 130° for oil-treated and 40° for untreated surfaces. The reported average *in situ* contact angels for the experimental data was 110% degrees [16] while experimental sessile drop data provided by Treiber et al. 1972 [12] reported contact angles up to 160% for carbonate rocks. It is well known that the wetting conditions depend on the oil used, acid number, and treatment method used to age the core [20]. It has also been shown that direct *in situ* contact angle measurements can under predict the true contact angle by up to 20 degrees at high contact angle values [21]. Therefore, a contact angle of 130% was our best educated guess at a representative value for both Models (1) and (2).

Table 1. Summary of the conducted simulations. The drainage saturation corresponds to the saturation at which surface wettability was assigned.

Simulation Name	Dataset	Wetting Model	Oil-Wet Fraction
CB_0.65_1	1	Cassie-Baxter	0.65
CB_0.84_1	1	Cassie-Baxter	0.84
CB_0.99_1	1	Cassie-Baxter	0.99
Uni_0.99_1_CA90	1	Uniform	0.99
Uni_0.99_2	2	Uniform	0.99

In total five simulations were conducted as summarised in Table 1. Region-of-interest (ROI) images of these simulations are provided in Figure 2. The oil phase renderings are ordered from water wet to oil wet. Also, an image pair (S_o = 0.5, S_o = 0.8) is presented for each simulation. The final image pair (k, l) is the experimental data. Firstly, we observe that oil

connectivity improves with increasing oil saturation. Secondly, the oil adheres to the solid surface in both models but much less so in the Cassie-Baxter model than the uniform model. Thirdly, the initial oil saturation used to mimic the core aging procedure clearly impacted the simulation results. Overall, the rendering in Figures 2i and 2j qualitatively reflect the oil morphologies observed in the experimental data. These renderings correspond to simulation Uni_0.99_2 (see Table 1), which reflects an oil-wet state with oil coating the grain surfaces.

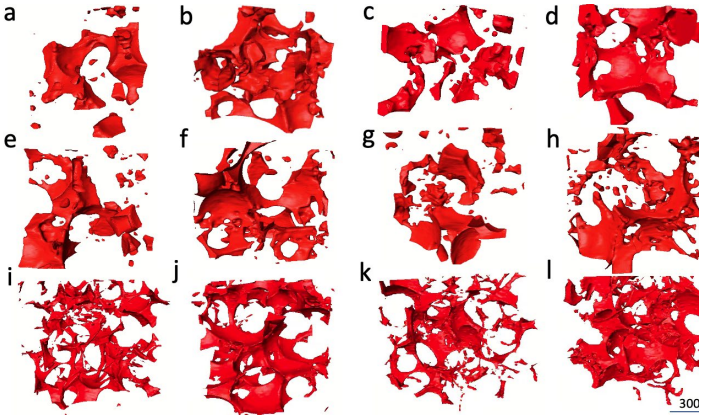

Fig. 2. Three-dimensional renderings of oil for five simulations and one experiment at oil saturations of 0.5 and 0.8; (a, b) are from simulation CB_0.65_1; (c, d) are from simulation CB_0.84_1; (e, f) are from simulation CB_0.99_1; (g, h) are from simulation Uni_0.99_1_CA90; (i, j) are from simulation Uni_0.99_2; and (k, l) are from the experimental data. See Table 1 for full details on each simulation case.

(a)

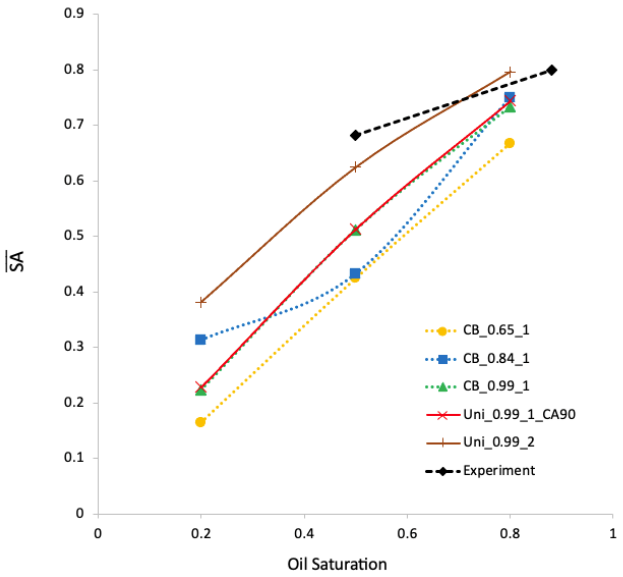

(b)

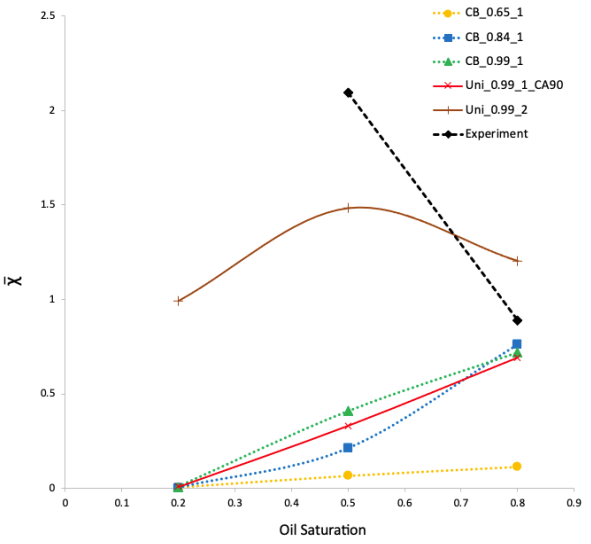

Fig. 3. (a) Surface area normalization (oil-grain surface area/total grain surface area (b) Euler normalization (Euler of NWP/Euler of pore space) of 5 simulations and experimental data. The reported value at oil saturation of 0.2 is not the residual oil saturation.

In Figure 3, we provide quantitative measures of the oil morphology. These measures were taken at the length scale of the simulations and experimental images, which were equivalent. The reported surface area values were determined by

$$\overline{SA} = \frac{M_1\left(\frac{oil}{grain}\right)}{M_1(grain)},$$

where $M_1(Grain)$ is the total surface area of all grain surfaces and $M_1\left(\frac{oil}{grain}\right)$ is only the oil-grain surface area. In this way, we measure surface area coverage following the work of [22]. The reported Euler characteristic values were determined by

$$\bar{\chi} = \chi(oil)/\chi(pore\ space),$$

where $\chi(oil)$ is the Euler characteristic of the oil phase and $\chi(pore\ space)$ is the Euler characteristic of the pore space. As oil fills the pore space, $\bar{\chi}$ approaches 1. For oil-wet cases, however, as observed by our simulation results and the experimental data, the oil phase can become more connected than the pore space, i.e., $\bar{\chi} > 1$. This occurs due to the oil forming multiple loops along the grain surfaces.

Overall, as observed in Figure 3, the results from simulation Uni_0.99_2 provided the best morphological comparison to the experimental data. While the morphological values do not provide an exact match with the experimental data the values are arguably similar, and the overall trends are captured. An exact match would not be expected given that the model domain and boundary conditions are not 1:1 with the experiment. This occurs because the flow outside of the experimentally imaged region is unknown.

Given a particular wetting state it would be expected that the fluid/fluid interfacial curvatures between simulation and experiment would be comparable. These curvature distributions are presented in Figure 4 for the experimental and Uni_0.99_2 simulation datasets. For the simulation, 20.54% of the mean curvature distribution falls outside of the mean curvature distribution that was experimentally measured. In addition, the sub-distributions of the Gaussian curvatures are qualitatively comparable between simulation and experiment. This further suggests that the wetting state was represented by the Uni_0.99_2 simulation.

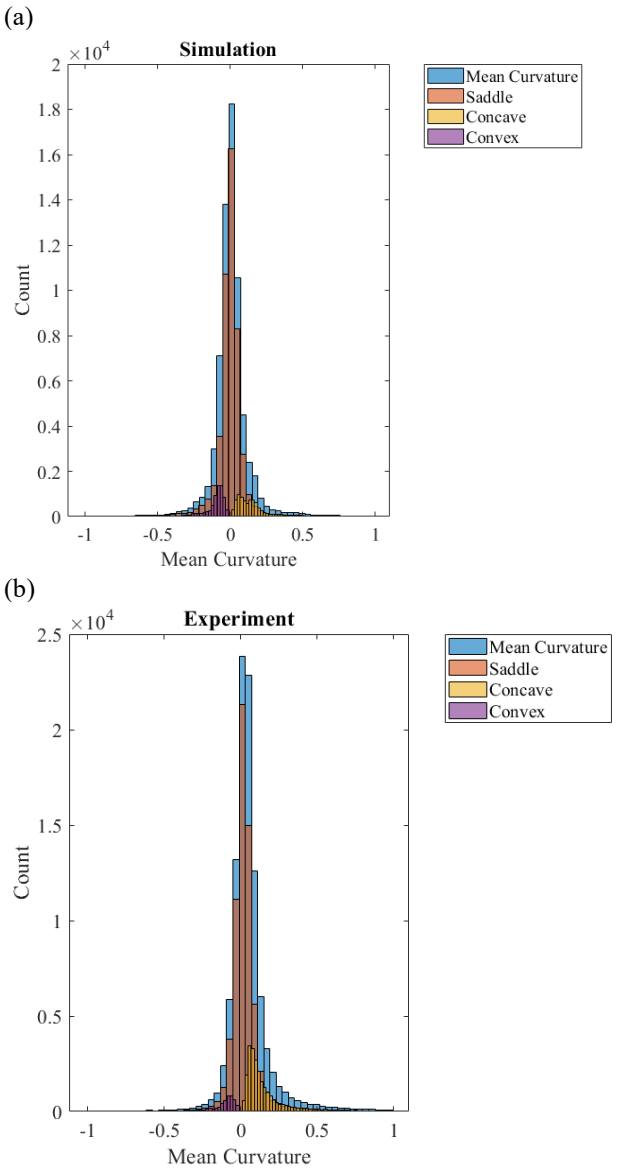

Fig. 4. (a) Curvature measurements of Uni_0.99_2 (So=0.50); (b) Curvature measurements of experimental data (So=0.50).

Overall, the simulation results suggested that a contact angle value of 130° for oil treated surfaces was representative of the experimental data while the Cassie-Baxter models created a too water-wet state. It can be assumed that the 130° uniform contact angle is an effective value and not the intrinsic contact angle of the surface, as defined by Young's equation, since the carbonate surface is clearly rough with a dual porosity system whereby the microporosity is below the image resolution. However, measuring the surface microporosity of the carbonate grains with micro-CT is problematic and knowing what value to use for θ_Y in Equation (3) is difficult.

The difficulty with measuring the microporosity of grain surfaces is demonstrated in Figure 5. Two distributions of microporosity are presented: (1) all values within 3 voxels from a grain surface and (2) all other voxel microporosity values. Due to the partial volume effect during imaging, the grain surface voxels have CT values preferentially less than those values within the grains [23]. This results in high micro-porosity on the grain surface, which in turn results in water-wet conditions when Equation (3) is applied. A better representation of the microporosity could be the average microporosity value of those voxels at least 3 voxels from the surface. Based on the distribution presented in Figure 5, the average microporosity value would be 0.1268.

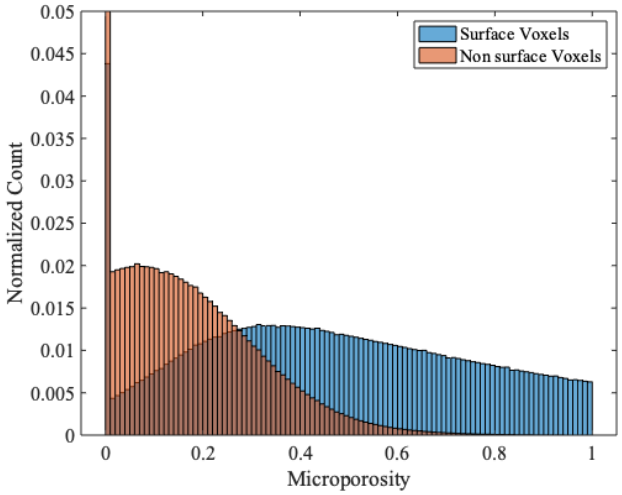

Fig. 5. Micro-porosity analysis. (1) Distribution of micro-porosity values for voxels that represent the grain surface. (2) Distribution of micro-porosity values that are at least 3 voxels from the surface.

An estimate of θ_Y can be obtained by using Equation (3). Based on simulation results, θ_E =130° provided the closes match to the experimental data. Based on Figure 5, the carbonate rock had an average microporosity of 0.1268. Therefore, θ_Y of the oil treated surfaces would have been approximately 160°. Such a contact angle is on the high-end of values reported by Treiber et al. 1972 [12] for oil treated pure (solid) calcite surfaces but remains within a reasonable range.

4. Conclusions

We conducted two-phase LBM simulations considering two different wetting models: (1) Uniform Wetting and (2) Cassie-Baxter Wetting. We then compared the resulting simulated morphological state of the oil to experimental data. Based on the oil phase images and morphological measures the Uni_0.99_2 model provided

the best approximation to the experimental data. This simulation case assumed a uniform contact angle of 130° for oil-treated and 40° for untreated surfaces. The experimental data was reported as being 'mixed-wet' even though the initial water saturation prior to imbibition was 0.1%. The impact that wettability heterogeneity could influence these results will need to be explored in future work.

We also highlighted the main difficulty with assigning surface wettability heterogeneity when working with micro-CT data. Due to the well-known partial volume effect, when applying Equation (2), surface voxels tend to have a lower solid fraction than expected based on solid fraction measurements taken far from an interface. Therefore, the Cassie-Baxter model resulted in more water-wet oil morphologies than that observed in the experimental data.

To best capture the wetting state, we provide the following suggestions for future work. Firstly, we should conduct more experiments with aging at different saturations. Secondly, we could consider dynamic aging by updating the contact angle values during the primary drainage process. Thirdly, we should consider the spatial distribution of the microporosity (at least three voxels from an interface) to assign a similar distribution to the model domain before applying the Cassie-Baxter model. This last suggestion would provide wettability heterogeneity to the surface and allow for a better understating to what degree this factor impacts the pore-scale morphology of oil.

References

[1] W. Abdallah *et al.*, "Fundamentals of wettability," *Technology*, vol. **38**, no. 1125–1144, p. 268, 1986.

[2] A. B. D. Cassie and S. Baxter, "Wettability of porous surfaces," *Trans. Faraday Soc.*, vol. **40**, p. 546, 1944, doi: 10.1039/tf9444000546.

[3] A. AlRatrout, M. J. Blunt, and B. Bijeljic, "Wettability in complex porous materials, the mixed-wet state, and its relationship to surface roughness," *Proc. Natl. Acad. Sci. U.S.A.*, vol. **115**, no. 36, pp. 8901–8906, Sep. 2018, doi: 10.1073/pnas.1803734115.

[4] Y. Y. Yan, Y. Q. Zu, and B. Dong, "LBM, a useful tool for mesoscale modelling of single-phase and multiphase flow," *Applied Thermal Engineering*, vol. **31**, no. 5, pp. 649–655, Apr. 2011, doi: 10.1016/j.applthermaleng.2010.10.010.

[5] E. Ezzatneshan and H. Vaseghnia, "Evaluation of equations of state in multiphase lattice Boltzmann method with considering surface wettability effects," *Physica A: Statistical Mechanics and its Applications*, vol. **541**, p. 123258, Mar. 2020, doi: 10.1016/j.physa.2019.123258.

[6] W. Anderson, "Wettability literature survey-part 2: Wettability measurement," *Journal of petroleum technology*, vol. **38**, no. 11, pp. 1–246, 1986.

[7] R. Zhang, N. Qin, L. Peng, K. Tang, and Z. Ye, "Wettability alteration by trimeric cationic surfactant at water-wet/oil-wet mica mineral surfaces," *Applied Surface Science*, vol. **258,** no. 20, pp. 7943–7949, Aug. 2012, doi: 10.1016/j.apsusc.2012.04.139.

[8] X. Zhou and N. R. Morrow, "Interrelationship of Wettability, Initial Water Saturation, Aging Time, and Oil Recovery by Spontaneous Imbibition and Waterflooding," *SPE Journal*, vol. **5**, no. 2, p. 9, 2000.

[9] E. Sripal and L. A. James, "Application of an Optimization Method for the Restoration of Core Samples for SCAL Experiments," p. 10, 2018.

[10] D. C. Standnes and T. Austad, "Wettability alteration in chalk 1. Preparation of core material and oil properties," p. 11, 2000.

[11] D. Y. Kwok and A. W. Neumann, "Contact angle measurement and contact angle interpretation," *Advances in Colloid and Interface Science*, vol. **81**, no. 3, pp. 167–249, Sep. 1999, doi: 10.1016/S0001-8686(98)00087-6.

[12] L. E. Treiber and W. W. Owens, "A Laboratory Evaluation of the Wettability of Fifty Oil-Producing Reservoirs," *Society of Petroleum Engineers Journal*, vol. **12**, no. 06, pp. 531–540, Dec. 1972, doi: 10.2118/3526-PA.

[13] W. G. Anderson, "Wettability Literature Survey-Part 1: Rock/Oil/Brine Interactions and the Effects of Core Handling on Wettability," *Journal of Petroleum Technology*, vol. **38**, no. 10, pp. 1125–1144, Oct. 1986, doi: 10.2118/13932-PA.

[14] Q. Lin, Y. Al-Khulaifi, M. J. Blunt, and B. Bijeljic, "Quantification of sub-resolution porosity in carbonate rocks by applying high-salinity contrast brine using X-ray microtomography differential imaging," *Advances in Water Resources*, vol. **96**, pp. 306–322, Oct. 2016, doi: 10.1016/j.advwatres.2016.08.002.

[15] A. M. Alhammadi, A. AlRatrout, K. Singh, B. Bijeljic, and M. J. Blunt, "In situ characterization of mixed-wettability in a reservoir rock at subsurface conditions," *Sci Rep*, vol. **7**, no. 1, p. 10753, Dec. 2017, doi: 10.1038/s41598-017-10992-w.

[16] A. Scanziani, K. Singh, T. Bultreys, B. Bijeljic, and M. J. Blunt, "In situ characterization of immiscible three-phase flow at the pore scale for a water-wet carbonate rock," *Advances in Water Resources*, vol. **121**, pp. 446–455, Nov. 2018, doi: 10.1016/j.advwatres.2018.09.010.

[17] A. Scanziani, Q. Lin, A. Alhosani, M. Blunt, and B. Bijeljic, "Dynamics of displacement in mixed-wet porous media," Engineering, preprint, Jan. 2020. doi: 10.31223/OSF.IO/JPMVC.

[18] J. E. McClure, Z. Li, M. Berrill, and T. Ramstad, "The LBPM software package for simulating multiphase flow on digital images of porous rocks," *Comput Geosci*, vol. **25**, no. 3, pp. 871–895, Jun. 2021, doi: 10.1007/s10596-020-10028-9.

[19] R. T. Armstrong *et al.*, "Porous Media Characterization Using Minkowski Functionals: Theories, Applications and Future Directions,"

Transp Porous Med, vol. **130**, no. 1, pp. 305–335, Oct. 2019, doi: 10.1007/s11242-018-1201-4.

[20] R. T. Armstrong, "Multiscale Characterization of Wettability in Porous Media," p. 26.

[21] C. Sun *et al.*, "Characterization of wetting using topological principles," *Journal of Colloid and Interface Science*, vol. **578**, pp. 106–115, Oct. 2020, doi: 10.1016/j.jcis.2020.05.076.

[22] G. Garfi, C. M. John, Q. Lin, S. Berg, and S. Krevor, "Fluid Surface Coverage Showing the Controls of Rock Mineralogy on the Wetting State," *Geophys. Res. Lett.*, vol. **47**, no. 8, Apr. 2020, doi: 10.1029/2019GL086380.

[23] D. Wildenschild and A. P. Sheppard, "X-ray imaging and analysis techniques for quantifying pore-scale structure and processes in subsurface porous medium systems," *Advances in Water Resources*, vol. **51**, pp. 217–246, Jan. 2013, doi: 10.1016/j.advwatres.2012.07.018.